Journal of Solid State Chemistry 183 (2010) 1239–1244

Contents lists available at ScienceDirect

Journal of Solid State Chemistry

journal homepage: www.elsevier.com/locate/jssc

One-dimensional NiCuZn ferrite nanostructures: Fabrication, structure, and magnetic properties

Jun Xiang [a,b], Xiangqian Shen [b,*], Fuzhan Song [b], Mingquan Liu [b]

[a] School of Mathematics and Physics, Jiangsu University of Science and Technology, Zhenjiang 212003, PR China
[b] School of Materials Science and Engineering, Jiangsu University, Zhenjiang 212013, PR China

ARTICLE INFO

Article history:
Received 12 January 2010
Received in revised form
25 March 2010
Accepted 30 March 2010
Available online 2 April 2010

Keywords:
NiCuZn ferrite
Nanofibers
Electrospinning
Magnetic properties

ABSTRACT

$Ni_{0.5-x}Cu_xZn_{0.5}Fe_2O_4$ ($0.0 \le x \le 0.5$) ferrite nanofibers with diameters of 80–160 nm have been prepared by electrospinning and subsequent heat treatment. Both the average grain size and lattice parameter are found to increase with the addition of copper. Fourier transform infrared spectra indicate that the portion of Fe^{3+} ions at the tetrahedral sites move to the octahedral sites as some of the substituted Cu^{2+} ions get into the tetrahedral sites. Vibrating sample magnetometer measurements show that the coercivity of these ferrite nanofibers decreases with increasing Cu concentration, whereas the specific saturation magnetization initially increases, reaches a maximum value at $x=0.2$ and then decreases with the Cu content further increase. Notable differences in magnetic properties at room temperature (298 K) and 77 K for the $Ni_{0.3}Cu_{0.2}Zn_{0.5}Fe_2O_4$ nanofibers and corresponding powders are observed and mainly arise from the grain size and morphological variations between these two materials.

© 2010 Elsevier Inc. All rights reserved.

1. Introduction

Ferrites are well-known commercially important functional materials because of their excellent magnetic and electrical properties [1]. Among various ferrite materials, the NiZn ferrites are considered as the most versatile soft magnetic materials due to their high resistivity and permeability and low eddy current loss for high frequency applications [2,3]. Guo et al. [4] prepared the NiZn ferrite thin films with well-crystallized spinel structure and thickness ~1.5 μm by radio frequency magnetron sputtering at room temperature on Si (1 1 1) substrates and found that all films exhibited very high resonance frequency exceeding Snoek's limit value of the corresponding ferrite bulk specimen. Zhao et al. [5] reported the fabrication process of NiZn spinel ferrite and Cu-doped, Co-doped NiZn spinel ferrite and their microwave absorbing properties, the results showed that all the prepared ferrite materials were good electromagnetic wave absorbers in the microwave range. The magnetic properties of NiZn ferrites are highly sensitive to grain size, microstructure, type and amount of additives, impurities, and the preparation routes [6]. Recently, various studies showed that the addition of copper in NiZn ferrites could tune the magnetic properties [7]. So that, the NiCuZn ferrites have been widely used to fabricate multilayer chip inductors (MLCI) and electromagnetic interference (EMI) filters [8,9]. Additionally, the NiCuZn ferrites have been also synthesized as a constituent of radar absorbing composite material [10]. As small particles with a high surface free energy are allowed to achieve a high density at low sintering temperatures, thus many researches focused on the preparation of NiCuZn ferrite nanoparticles by various wet chemical routes such as hydrothermal [11], sol–gel [12], and co-precipitation [13]. However, to the best of our knowledge up to now, the NiCuZn ferrite in a nanofiber form has not been reported in literatures. Compared to other NiCuZn ferrite nanostructures, the unique structural characteristics (e.g., shape anisotropy and high aspect ratios) of NiCuZn ferrite nanofibers are beneficial not only to enhance the permeability and resonance frequency, but also to improve the mechanical properties of polymer matrix composite materials in specific fields of application.

Recently, one-dimensional (1D) magnetic nanostructured materials have been investigated intensively due to their novel chemical and physical properties and their potential as building blocks for next-generation electromagnetic devices [14,15]. As compared to other methods [16], the electrospinning technique has been proved to be a simple and versatile method for manufacturing 1D structural materials [17,18]. A variety of materials, such as polymers [19], metal [20], metal oxides [17], and hybrid (organic/inorganic) nanofibers [21] have been prepared using electrospinning method. Some spinel ferrite 1D nanostructures (e.g., nanofibers and nanoribbons) with a general formula MFe_2O_4 (M=Co, Ni, Zn, Mn, Cu, Mg, etc.) were also synthesized by an eletrospinning process [22–27]. The aim of the present work is to fabricate NiCuZn ferrite nanofibers using sol–gel process and electrospinning, investigate the effect of Cu^{2+} ions

* Corresponding author. Fax: +86 511 88791964.
E-mail address: shenxq@ujs.edu.cn (X. Shen).

0022-4596/$ - see front matter © 2010 Elsevier Inc. All rights reserved.
doi:10.1016/j.jssc.2010.03.041

substitution on the structure, morphology, and magnetic properties of the resulting nanofibers with composition of $Ni_{0.5-x}Cu_xZn_{0.5}Fe_2O_4$ ($0.0 \le x \le 0.5$). Also, the magnetic properties at room temperature (298 K) and 77 K of the as-prepared $Ni_{0.3}Cu_{0.2}Zn_{0.5}Fe_2O_4$ nanofibers are compared with that of the counterpart nanoparticles prepared by a conventional sol–gel method.

2. Experimental section

The preparation of $Ni_{0.5-x}Cu_xZn_{0.5}Fe_2O_4$ ($0.0 \le x \le 0.5$) nanofibers is similar to the process described in our previous paper [28,29] and consisted of solution preparation, electrospinning and calcination. In a typical procedure, 0.47 g of poly (vinyl pyrrolidone) (PVP, Mw ≈ 1,300,000, Aldrich) was dissolved in mixture of ethanol (4.53 g) and distilled water (2.0 g), followed by magnetic stirring for 1 h to ensure the dissolution of PVP. Then appropriate amount of nickel acetate [$Ni(CH_3COO)_2 \cdot 4H_2O$, AR], copper acetate [$Cu(CH_3COO)_2 \cdot H_2O$, AR], zinc acetate [($Zn(CH_3COO)_2 \cdot 2H_2O$), AR], and ferric nitrate [($Fe(NO_3)_3 \cdot 9H_2O$), AR] with $0.5-x$:x:0.5:2 molar ratios of Ni:Cu:Zn:Fe were added into the PVP/ethanol/water solution and further magnetically stirred for about 20–24 h at room temperatures to form a homogeneous viscous solution with PVP concentration of 6 wt% for electrospinning. The viscous solution was loaded into a plastic syringe with a stainless steel needle. The needle used as the positive electrode was connected to a high-voltage supply and the solution was fed at a rate of 0.5 mL/h using a syringe pump during the electrospinning process. A piece of aluminum foil used as the ground collector was placed in front of the needle tip to collect the composite fibers. The distance between syringe needle tip and collector was 15 cm and the applied voltage was 15 kV. The as-spun $Ni_{0.5-x}Cu_xZn_{0.5}Fe_2O_4$/PVP composite fibers collected were dried and calcined at 600 °C for 2 h in ambient atmosphere to obtain the resulting nanofibers. For comparison, $Ni_{0.3}Cu_{0.2}Zn_{0.5}Fe_2O_4$ powders were also prepared using a conventional sol–gel process, in which the precursor was obtained by complexation of metal salt and citric acid, followed by drying and then calcination in air at 600 °C for 2 h.

The X-ray diffraction (XRD) patterns were collected on a Rigaku D/max 2500PC diffractometer with Cu$K\alpha$ radiation. Fourier transform infrared spectroscopy (FT-IR) spectra of the samples (as pellets in KBr) were recorded by a Nicolet Avatar 370 spectrometer in a wavenumber range of 375–4000 cm^{-1} at a resolution of 2 cm^{-1}. Field emission scanning electron microscopy (FE-SEM, JSM-7001F) equipped with an Oxford INCA energy-dispersive X-ray (EDX) spectrometer and transmission electron microscopy (TEM, JEM-2100) were employed to analyze the morphology, chemical composition and microstructure of the samples. The magnetic properties of the as-prepared nanofibers and powders were investigated at room temperature (298 K) and 77 K (in liquid nitrogen) using a vibrating sample magnetometer (VSM, HH-15).

3. Results and discussion

X-ray diffraction patterns of $Ni_{0.5-x}Cu_xZn_{0.5}Fe_2O_4$ nanofibers obtained by calcining the corresponding polymer/inorganic composite fibers at 600 °C for 2 h are shown in Fig. 1. As can be seen from Fig. 1, the patterns match well the characteristic diffraction peaks of NiZn ferrites (JCPDS card no. 08-0234) and do not change obviously with the increase of Cu content, thus, confirming the formation of single-phase cubic spinel structure. The average grain size of nanofibers was calculated from the XRD

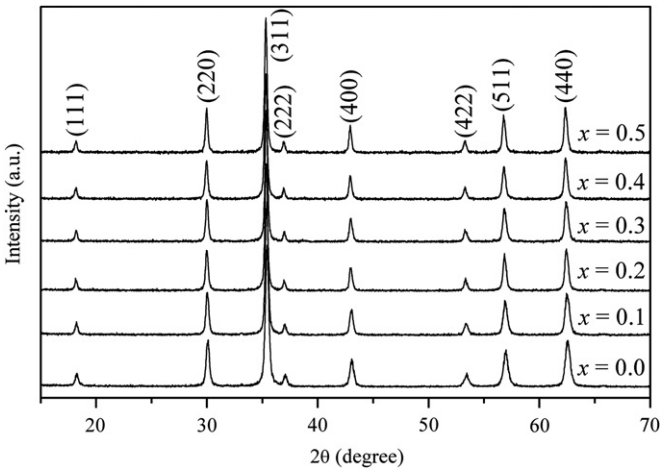

Fig. 1. X-ray diffraction patterns of $Ni_{0.5-x}Cu_xZn_{0.5}Fe_2O_4$ nanofibers calcined at 600 °C for 2 h.

Table 1
Lattice parameter (a) and mean grain size (D) calculated from XRD spectra and FT-IR characteristic frequencies (ν_1, ν_2) of $Ni_{0.5-x}Cu_xZn_{0.5}Fe_2O_4$ nanofibers calcined at 600 °C for 2 h.

x in $Ni_{0.5-x}Cu_xZn_{0.5}Fe_2O_4$	a (Å)	D (nm)	ν_1 (cm^{-1})	ν_2 (cm^{-1})
0.0	8.4019(8)	26.5(5)	574.2	390.2
0.1	8.4090(12)	32.4(3)	572.8	391.8
0.2	8.4142(10)	36.6(4)	570.8	395.1
0.3	8.4181(10)	39.7(4)	567.0	388.6
0.4	8.4201(4)	42.1(7)	563.1	386.6
0.5	8.4237(13)	44.6(5)	557.4	390.6

line broadening of the (3 1 1) peak using the Scherrer equation. The estimated mean grain size increases gradually with increasing Cu content as presented in Table 1. The observed increase in grain size with Cu content is due to a higher mobility of Cu^{2+} ions induced by liquid phase sintering. The values of lattice parameter (a) obtained by fitting the diffraction peaks using standard least-squares method are also given in Table 1. The lattice parameter increases from 8.4019(8) to 8.4237(13)Å along with the substitution of Cu^{2+} ions for Ni^{2+} ions. This is due to the fact that Cu^{2+} ions have a larger ionic radius (0.87 Å) than Ni^{2+} ions (0.83 Å) [30].

Fig. 2 shows the FT-IR spectra of the $Ni_{0.5-x}Cu_xZn_{0.5}Fe_2O_4$ nanofibers calcined at 600 °C for 2 h, which further helps elucidating the formation of the spinel structure in the NiCuZn ferrite nanofibers. The FT-IR spectra of all the samples show prominent bands at 3450 and 1635 cm^{-1} which are attributed to the stretching mode and H–O–H bending vibration of water absorbed by the nanofibers due to their high surface area to volume ratio. The weak band at 1384 cm^{-1} is ascribed to asymmetric NO_3^- stretching vibration arising from the residual nitrate groups. The retention of water and NO_3^- groups, up to 600 °C, has also been reported in some nanostructural materials [3,31,32]. The two strong absorption bands in the range 557–575 and 386–395 cm^{-1} are characteristic bands of spinel ferrite and can be assigned to the vibrations of the metal ion–oxygen complexes in the tetrahedral (A) and octahedral (B) sites, respectively [3]. The vibration frequencies ν_1 and ν_2, respectively, corresponding to A and B sites for the as-prepared $Ni_{0.5-x}Cu_xZn_{0.5}Fe_2O_4$ nanofibers are given in Table 1.

It is known that in spinel ferrite systems, Ni^{2+} ions show a strong preference to B sites while Zn^{2+} ions have a strong preference for A sites, and Cu^{2+} ions can exit at both the sites

though they prefer to occupy *B* sites. It can be seen from Fig. 2 and Table 1 that the value of ν_1 shifts slightly to lower wavenumber with the increase of Cu content, which suggests that some of the Cu^{2+} ions may tend to occupy *A* sites and the quantity of Cu^{2+} ions in *A* sites gradually increase with increasing substitution of Cu^{2+} ions for Ni^{2+} ions in the NiZn ferrite. This can be explained on the basis of the distribution of cations. If the Cu^{2+} ions introduced in the system enter *A* sites, this will push the Fe^{3+} ions to move from *A* into *B* sites, thereby leading to the decrease of tetrahedral vibration frequency as the Cu^{2+} ions with a larger ionic radius and greater atomic weight than Fe^{3+} ions at *A* sites. On the other hand, when the Cu^{2+} ions replace Ni^{2+} ions with comparatively smaller radius and lower atomic weight at *B* sites, the ν_2 also ought to shifts to lower wavenumber. However, the obtained FT-IR spectral data show that the octahedral vibration frequency (ν_2) only have a slight and irregular displacement, which may be related to the migration of Fe^{3+} ions from *A* to *B* sites as mentioned above.

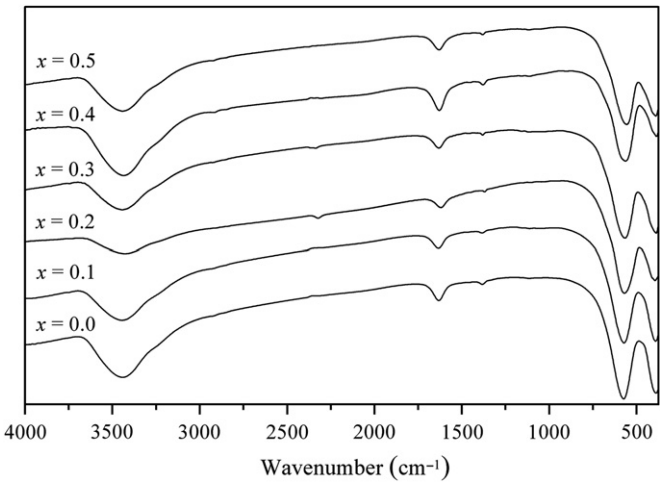

Fig. 2. FT-IR spectra of $Ni_{0.5-x}Cu_xZn_{0.5}Fe_2O_4$ nanofibers.

Fig. 3 shows the SEM images of $Ni_{0.5-x}Cu_xZn_{0.5}Fe_2O_4$ nanofibers with different Cu contents calcined at 600 °C for 2 h. It can be observed that the Cu content has no remarkable influences on the morphologies of the nanofibers. As the PVP is selectively burned out during calcination of the as-spun composite nanofibers in air at 600 °C, the nanofibers still maintain a continuous structure. Each individual nanofiber is uniform in cross-section, and the diameters of these nanofibers range from 80 to160 nm.

In order to confirm the chemical composition of as-prepared $Ni_{0.5-x}Cu_xZn_{0.5}Fe_2O_4$ nanofibers, a quantitative elemental analysis on these samples was carried out by the energy-dispersive X-ray spectrometer attached to the scanning electron microscope. Fig. 4 shows the EDX spectra of the obtained $Ni_{0.5-x}Cu_xZn_{0.5}Fe_2O_4$ nanofibers, and the corresponding elemental analysis results are listed in Table 2. The results indicate that the atomic percentage (at%) of Ni, Cu, Zn, and Fe in the $Ni_{0.5-x}Cu_xZn_{0.5}Fe_2O_4$ nanofibers determined by EDX basically agree with the designed composition.

Fig. 5(a) shows a TEM image of the $Ni_{0.3}Cu_{0.2}Zn_{0.5}Fe_2O_4$ nanofibers after calcination at 600 °C, indicating that the nanofibers are built from $Ni_{0.3}Cu_{0.2}Zn_{0.5}Fe_2O_4$ nanoparticles with domain sizes around 38 ± 5 nm, this value is consistent with the average crystallite size (~36.6 nm) estimated from the XRD peaks using the Scherrer formula. In comparison, the TEM image and XRD pattern of the $Ni_{0.3}Cu_{0.2}Zn_{0.5}Fe_2O_4$ powders prepared using the conventional sol–gel process are shown in Figs. 5(b) and (c), respectively. The average crystallite size for the powders is 48 ± 8 and 44 ± 2 nm, as estimated by TEM and XRD, respectively, which is bigger than that of the nanoparticles which build the nanofibers.

The magnetization hysteresis loop measurements were made to determine the specific saturation magnetization (M_s) and coercivity (H_c). In Fig. 6 the M_s and H_c at room temperature estimated from the $M(H)$ loops of $Ni_{0.5-x}Cu_xZn_{0.5}Fe_2O_4$ nanofiber samples are plotted as a function of Cu content. It can be seen

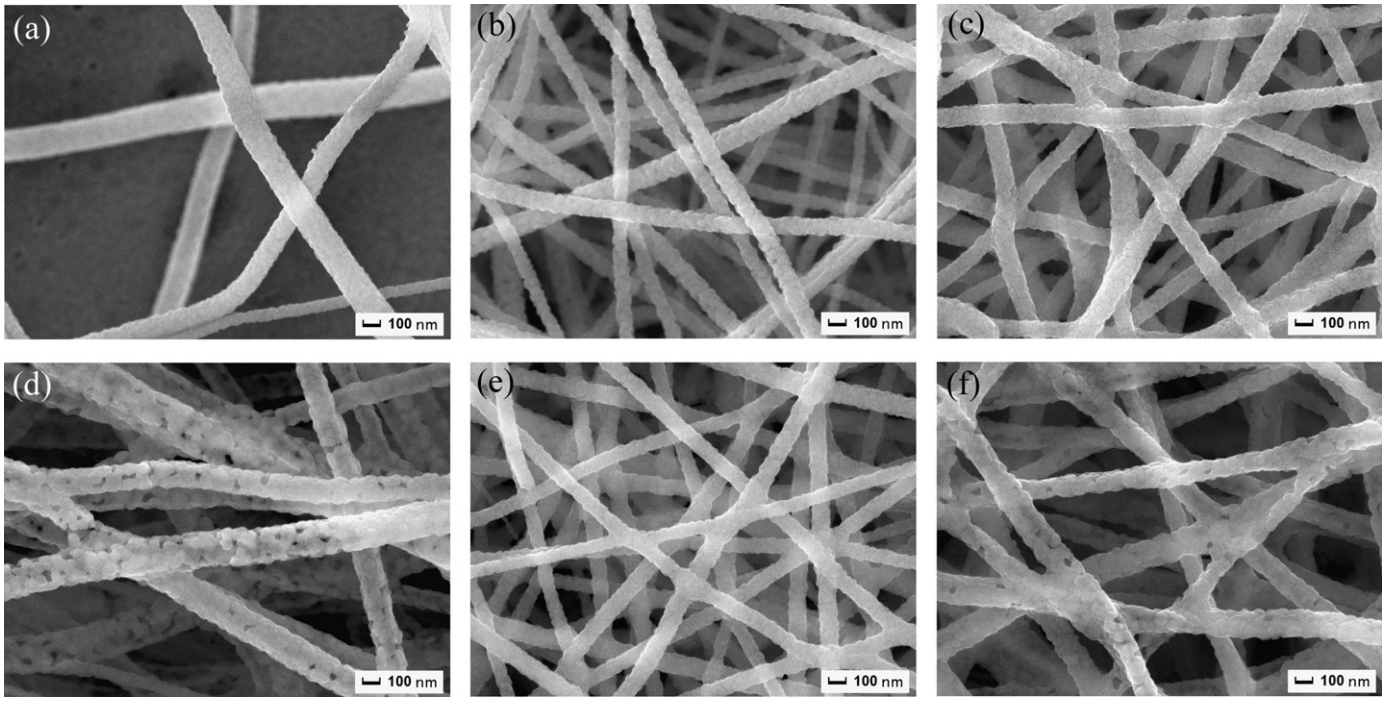

Fig. 3. SEM images of $Ni_{0.5-x}Cu_xZn_{0.5}Fe_2O_4$ nanofibers with different Cu contents (x): (a) 0.0; (b) 0.1; (c) 0.2; (d) 0.3; (e) 0.4 and (f) 0.5.

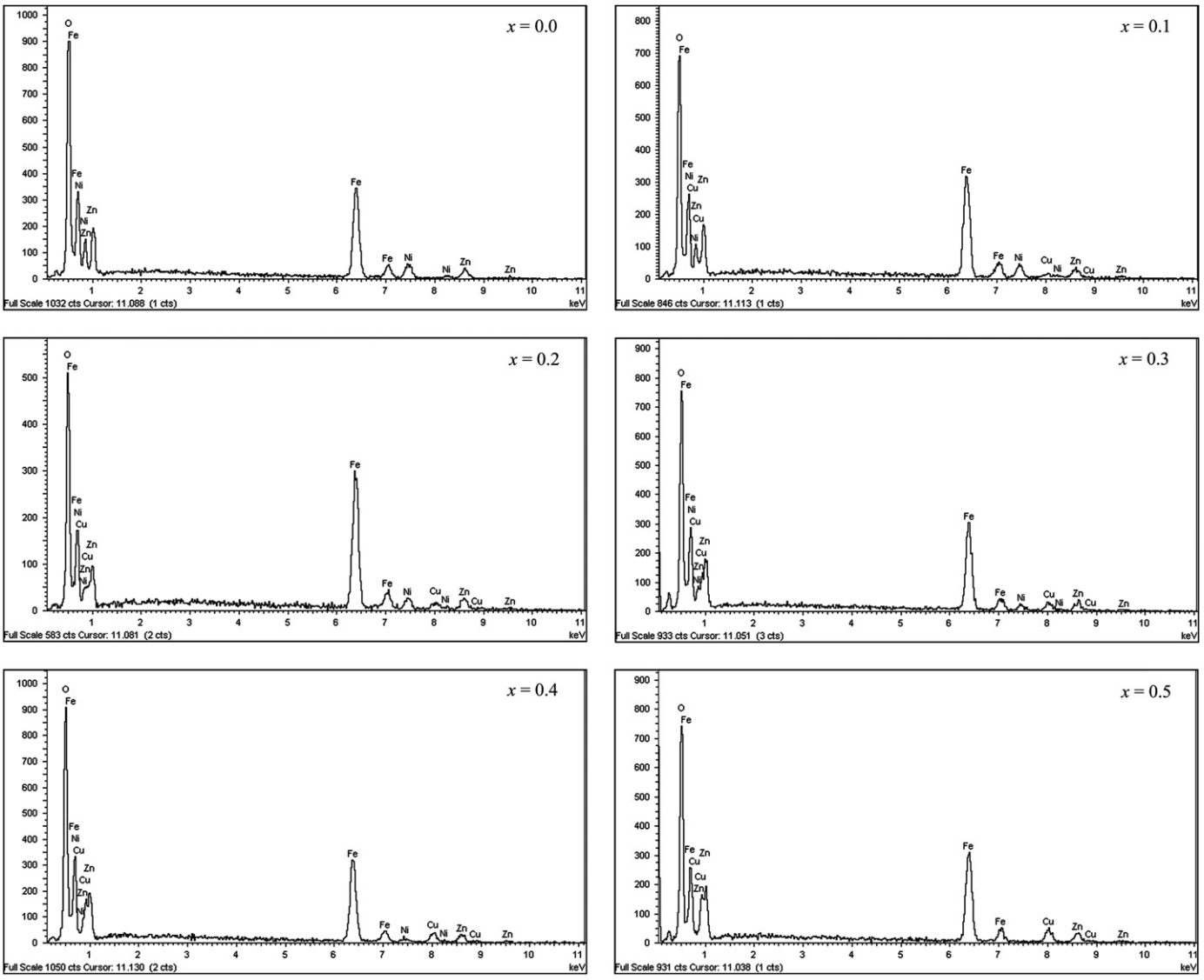

Fig. 4. EDX spectra of $Ni_{0.5-x}Cu_xZn_{0.5}Fe_2O_4$ nanofibers.

Table 2
The EDX elemental analysis results of as-prepared $Ni_{0.5-x}Cu_xZn_{0.5}Fe_2O_4$ nanofibers.

x in $Ni_{0.5-x}Cu_xZn_{0.5}Fe_2O_4$	Elemental compositions (at%)			
	Ni	Cu	Zn	Fe
0.0	6.79	—	7.69	26.80
0.1	6.13	1.65	7.76	30.97
0.2	4.52	3.13	7.64	29.47
0.3	2.84	4.65	7.74	27.06
0.4	1.42	5.92	7.03	26.58
0.5	—	7.80	7.84	28.15

from Fig. 6 that the coercivity at room temperature for the nanofibers shows a continuous reduction with increasing Cu^{2+} ions substitution. This coercivity reduction may be attributed to the lower magnetocrystalline anisotropy of Cu^{2+} ions as compared to Ni^{2+}. The replacement of Ni^{2+} ions by Cu^{2+} ions in the ferrite will result in a decrease in the coercivity value according to the Stoner–Wolfforth model ($H_c \sim 2K/M_s$) [33].

For M_s, however, its value increases initially and then decreases with the copper content. A similar variable trend of magnetization with Cu^{2+} ions doping has been reported by Dimri et al. [34] as well. The variation of M_s with composition can be explained on the basis of the exchange interaction between the ions at the tetrahedral (A) and octahedral (B) sites in the lattice. According to Neel's theory [35], the molecular magnetization (M) is given by the difference between the magnetizations M_B and M_A of the octahedral and tetrahedral sublattices, respectively, where the B sublattice generally has a higher magnetization. As Cu^{2+} ions have a lower magnetic moment ($1\,\mu_B$) than Ni^{2+} ions ($2\,\mu_B$), consequently, the substitution of Cu^{2+} ions for Ni^{2+} ions in the octahedral sites should result in a decrease in saturation magnetization. However, the experimental result indicate that M_s values show an increase with increasing Cu content when the Cu content at a low concentration ($x \leq 0.2$). This is attributed to the fact that some of the substituted Cu^{2+} ions occupy A sites as evidenced by the previous FT-IR analysis. In this case, a fraction of Fe^{3+} ions originally present at A sites are forced to migrate to B sites. This cation distribution will increase the magnetic moment of B sublattice and simultaneously result in a decrease in that of A sublattice, as the Fe^{3+} ions have a higher magnetic moment ($5\,\mu_B$)

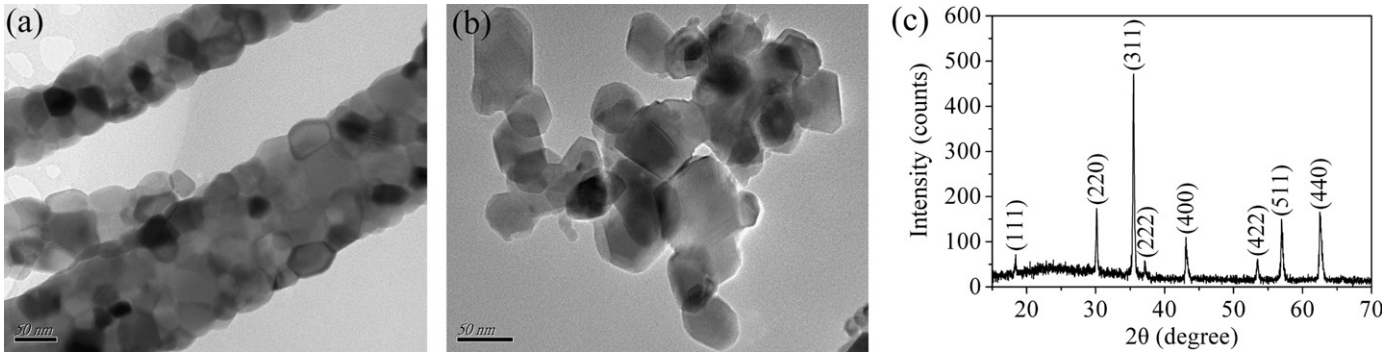

Fig. 5. TEM images of: (a) $Ni_{0.3}Cu_{0.2}Zn_{0.5}Fe_2O_4$ nanofibers; (b) powders and (c) XRD pattern of $Ni_{0.3}Cu_{0.2}Zn_{0.5}Fe_2O_4$ powders.

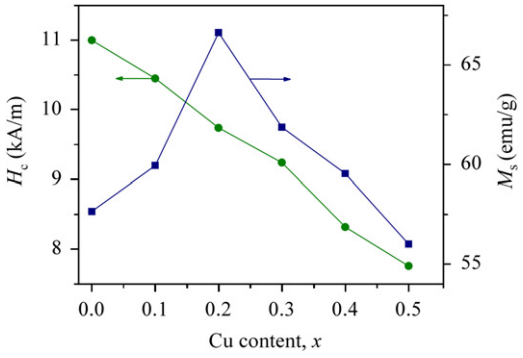

Fig. 6. Variation of specific saturation magnetization (M_s) and coercivity (H_c) with Cu content for $Ni_{0.5-x}Cu_xZn_{0.5}Fe_2O_4$ nanofibers at room temperature.

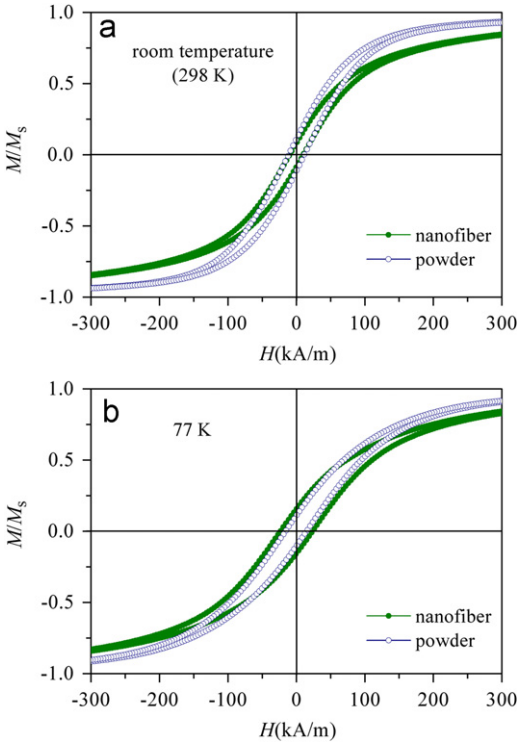

Fig. 7. M–H loops of $Ni_{0.3}Cu_{0.2}Zn_{0.5}Fe_2O_4$ nanofibers and powders (a) at room temperature (298 K) and (b) at 77 K.

than the Cu^{2+} ions. Thus, the net magnetic moment per molecule is increased, leading to the enhancement of M_s.

With a further substitution of Ni^{2+} ions by Cu^{2+} ions, on the one hand, more Cu^{2+} ions get into *A* sites, and more Fe^{3+} ions are forced to migrate to *B* sites. This will weak the *A*–*B* exchange interaction and enhance the *B*–*B* exchange interaction, which is predominantly present in zinc rich ferrite, and consequently permit the anti-parallel spin coupling and result in a decrease in the magnetic moment of *B* sublattice. On the other hand, at a high Cu content the majority of Cu^{2+} ions introduced into the spinel lattice still occupy *B* sites, which will reduce the magnetic moment of *B* sublattice, as the magnetic moment of Cu^{2+} ions is less than that of Ni^{2+} ions. Hence the reduction in the specific saturation magnetization for $Ni_{0.5-x}Cu_xZn_{0.5}Fe_2O_4$ nanofibers is observed when the Cu content x is over 0.2.

Vibrating sample magnetometer measurements imply that the magnetic behavior of $Ni_{0.3}Cu_{0.2}Zn_{0.5}Fe_2O_4$ (as an example of the studied compounds) nanofibers is different from that of the corresponding powder sample prepared using the conventional sol–gel method. Fig. 7 shows the magnetization curves for both nanofiber and powder samples. At room temperature (Fig. 7(a)), the coercivity of the nanofiber and powder samples is 9.7 and 11.6 kA/m, respectively. It is well known that the magnetic properties of a magnetic material depend largely on its grain size and morphology. The coercivity of magnetic particles decreases with particle size when the dimension is less than the critical size of single-domain (for $Ni_{0.5}Zn_{0.5}Fe_2O_4$ and $Cu_{0.5}Zn_{0.5}Fe_2O_4$ nanoparticles, this value is around 60 and 100 nm, respectively [36,37]). As shown by TEM and XRD studies, the powder sample has a larger mean particle size and therefore a larger coercivity at room temperature. Whilst at 77 K (Fig. 7(b)), the nanofiber sample exhibits a coercivity of 23.6 kA/m, which is higher than that (15.4 kA/m) of the powder sample. A similar behavior has been observed for $NiFe_2O_4$ nanofiber and powder samples [22]. Li et al. believed that the relatively large coercivity of nanofibers at low temperature was primarily due to their morphology. The theory has predicted that a system containing magnetic dipoles that are arranged into a linear chain will exhibit an increase in coercivity [38]. In our case, the experimental results also indicate that the dipole–dipole interactions between grains may play a dominant role in the magnetization process for the $Ni_{0.3}Cu_{0.2}Zn_{0.5}Fe_2O_4$ nanofibers. Under this interaction, all magnetic dipoles in the nanofibers tend to line up along the same axis. As described in Ref. [22], at low temperature, because the influence of thermal fluctuation on the rotation of magnetic dipoles is much reduced, a higher magnetic field strength is required to reverse the magnetization direction of these aligned dipoles, which result in a larger coercivity for the nanofibers. However, at high temperature the thermal agitation dominates over dipole–dipole interactions and tends to randomize magnetic dipoles. Therefore, this enhancement effect is not observed at room temperature.

4. Conclusions

The present work reports the structure and magnetic properties of the NiCuZn ferrite nanofibers prepared by electrospinning technique and analyses differences in magnetic properties at room temperature and 77 K between the nanofibers and the powders prepared by the conventional sol–gel process. All the resultant nanofibers calcined at 600 °C have a cubic spinel structure and a diameter ranging from 80 to 160 nm. The addition of copper promotes the grain growth, with an expanded lattice and modified cation distribution. The lattice parameter is found to increase with increasing Cu content due to a larger ionic radius of Cu^{2+} ions compared with that of Ni^{2+} ions. The FT-IR data suggest that some of the substituted Cu^{2+} ions tend to occupy *A* sites and force the same portion of Fe^{3+} ions to migrate from *A* to *B* sites. With the increase of Cu content, the coercivity of the nanofibers decreases due to a lower magnetocrystalline anisotropy of Cu^{2+} ions as compared to Ni^{2+} ions. However, the specific saturation magnetization initially increases, reaches a maximum value at $x=0.2$ and then decreases, which can be explained on the basis of the cation distribution and exchange interaction in the ferrite lattice. In addition, it is notable that obvious differences in magnetic properties at room temperature and 77 K for the $Ni_{0.3}Cu_{0.2}Zn_{0.5}Fe_2O_4$ nanofibers and corresponding powders mainly arise from the grain size and morphological variations between these two materials.

Acknowledgments

This work was supported by the National Natural Science Foundation of China (Grant no. 506740482), the Jiangsu Province's Postgraduate Cultivation and Innovation Project (Grant no. CX09B-192Z) and the Young Key Teachers Program of Jiangsu University of Science and Technology.

References

[1] M. Sugimoto, J. Am. Ceram. Soc. 82 (1999) 269.
[2] M.A. Gabal, Y.M. Al Angari, Mater. Chem. Phys. 115 (2009) 578.
[3] P. Priyadharsini, A. Pradeep, P. Sambasiva Rao, G. Chandrasekaran, Mater. Chem. Phys. 116 (2009) 207.
[4] D.W. Guo, Z.M. Zhang, M. Lin, X.L. Fan, G.Z. Chai, J. Phys. D 42 (2009) 125006.
[5] D.L. Zhao, Q. Lv, Z.M. Shen, J. Alloys Compd. 480 (2009) 634.
[6] M. Kaiser, J. Alloys Compd. 468 (2009) 15.
[7] H. Su, H.W. Zhang, X.L. Tang, Z.Y. Zhong, Y.L. Jing, Mater. Sci. Eng. B 162 (2009) 22.
[8] H. Su, H.W. Zhang, X.L. Tang, Y.L. Liu, J. Mater. Sci. 42 (2007) 2849.
[9] F. Liu, C. Yang, T.L. Ren, A.Z. Wang, J. Yu, L.T. Liu, J. Magn. Magn. Mater. 309 (2007) 75.
[10] U.R. Lima, M.C. Nasar, R.S. Nasar, M.C. Rezende, J.H. Araújo, J.F. Oliveira, Mater. Sci. Eng. B 151 (2008) 238.
[11] Y.P. Fu, J. Am. Ceram. Soc. 89 (2006) 3547.
[12] P.A. Jadhav, R.S. Devan, Y.D. Kolekar, B.K. Chougule, J. Phys. Chem. Solids 70 (2009) 396.
[13] J.S. Kim, C.W. Ham, Mater. Res. Bull. 44 (2009) 633.
[14] L.Y. Zhang, Y.F. Zhang, J. Magn. Magn. Mater. 321 (2009) L15.
[15] L. Luo, B.D. Sosnowchik, L.W. Lin, Appl. Phys. Lett. 90 (2007) 093101.
[16] Y. Xia, P. Yang, Y. Sun, Y. Wu, B. Mayers, B. Gates, Y. Yin, F. Kim, H. Yan, Adv. Mater. 15 (2003) 353.
[17] D. Li, J.T. McCann, Y.N. Xia, J. Am. Ceram. Soc. 89 (2006) 1861.
[18] A. Greiner, J.H. Wendorff, Angew. Chem. Int. Ed. 46 (2007) 5670.
[19] J.D. Schiffman, C.L. Schauer, Polym. Rev. 48 (2008) 317.
[20] J.L. Shui, J.C.M. Li, Nano Lett. 9 (2009) 1307.
[21] X. Lu, C. Wang, Y. Wei, Small 5 (2009) 2349.
[22] D. Li, T. Herricks, Y.N. Xia, Appl. Phys. Lett. 83 (2003) 4586.
[23] Y.W. Ju, J.H. Park, H.R. Jung, S.J. Cho, W.J. Lee, Compos. Sci. Technol. 68 (2008) 1704.
[24] W. Ponhan, S. Maensiri, Solid State Sci. 11 (2009) 479.
[25] J.H. Nam, Y.H. Joo, J.H. Lee, J.H. Chang, J.H. Cho, M.P. Chun, B.I. Kim, J. Magn. Magn. Mater. 321 (2009) 1389.
[26] Z.L. Wang, X.J. Liu, M.F. Lv, P. Chai, Y. Liu, J. Meng, J. Phys. Chem. B 112 (2008) 11292.
[27] S. Maensiri, M. Sangmanee, A. Wiengmoon, Nanoscale Res. Lett. 4 (2009) 221.
[28] J. Xiang, X.Q. Shen, F.Z. Song, M.Q. Liu, Chin. Phys. B 18 (2009) 4960.
[29] J. Xiang, X.Q. Shen, F.Z. Song, X.F. Meng, Chin. Phys. Lett. 27 (2010) 017502.
[30] R.D. Shannon, Acta Crystallogr. A 32 (1976) 751.
[31] K.H. Wu, T.H. Ting, C.I. Liu, C.C. Yang, J.S. Hsu, Compos. Sci. Technol. 68 (2008) 132.
[32] H.W. Yan, K. Zhang, C.F. Blanford, L.F. Francis, A. Stein, Chem. Mater. 13 (2001) 1374.
[33] K. Maaz, W. Khalid, A. Mumtaz, S.K. Hasanain, J. Liu, J.L. Duan, Physica E 41 (2009) 593.
[34] M.C. Dimri, A. Verma, S.C. Kashyap, D.C. Dube, O.P. Thakur, C. Prakash, Mater. Sci. Eng. B 133 (2006) 42.
[35] L. Neel, Ann. Phys. 3 (1948) 137.
[36] Y. Liu, T. Qin, Chin. Phys. 16 (2007) 3837.
[37] P. Chand, Hyperfine Interact. 184 (2008) 195.
[38] I.S. Jacobs, C.P. Bean, Phys. Rev. 100 (1955) 1060.